Proton energy spectra from ultra-intense laser interactions with film targets of varying thicknesses

C. Palmer, C. Bellei, A. E. Dangor, S. Kneip, S. P. D. Mangles, S. R. Nagel, Z. Najmudin and L. Willingale
Blackett Laboratory, Imperial College London, London SW7 2BZ, UK

R. J. Clarke and R. Heathcote
Central Laser Facility, STFC, Rutherford Appleton Laboratory, HSIC, Didcot, Oxon OX11 0QX, UK

A. Henig and J. Schreiber
Max-Planck Institut für Quanten Optik, Garching, Germany

M. C. Kaluza and A. Sävart
Institut für Quantenelektronik, Freidrick-Schiller-Universitat, Jena, Germany

Contact | c.palmer07@imperial.ac.uk

Introduction

Ion acceleration is an important and interesting branch of physics with a large number of applications. The development of chirped pulse amplification (CPA) techniques have made possible the production of high intensity, short duration laser pulses which can be used to generate energetic beams of ions [1], by interaction with a target, over much shorter distances than conventional accelerators.

High-intensity lasers can be used to create electric fields of MV/μm within a plasma, resulting from space charge separation of hot electrons. Ions accelerated by these high electric fields can potentially be used for a large number of applications: as a probe for high-density plasmas [2], for imaging and treatment of cancerous tumors [3] as well as as a compact ion source for the production of isotopes [4]. A large number of proposed applications require the ion beams to have a high energy with a low energy spread and a low divergence. These properties have a sensitive dependence on the acceleration mechanism and usually generated beams have a broad energy spectrum and divergence of ~40°. Different methods of energy selection have been shown to generate quasi-monoenergetic ion beams, both experimentally and theoretically [5,6], however, in the case discussed here basic acceleration mechanisms were considered.

One such mechanism is that of electrostatic shocks, produced at the front surface of the target [7]. Shocks result from a pressure imbalance between the radiation pressure of the laser and the plasma pressure. The laser pressure is due to the ponderomotive force which pushes electrons from higher to lower intensity regions. The ion motion, due to this force, is much less than that of the electrons due to their significantly lower charge to mass ratio, however, the ions respond to the space charge separation generated by the movement of the electrons. This in turn leads to a density perturbation which propagates through the target and is capable of accelerating ions to twice the shock velocity. For thinner targets higher ion energies can be reached as the shock wave has a higher absolute speed. Ponderomotive expulsion of electrons from the surface plasma also results in a strong electric field which can accelerate the remaining ions [7]. However, the majority of measured ions are accelerated from the rear surface.

Electrons, within the underdense preplasma created at the front surface of the target by the prepulse, gain thermal energy through interaction with the electric field of the laser via vacuum heating [8] and resonance heating [9]. Both mechanisms are minimised for normal incidence, with optimum absorption in cases with approximately 45° between the incident laser axis and target normal. At high intensities the dominant mechanism for normally incident laser pulses is J×B heating [9,10]. This is due to the oscillating component of the Lorentz force and is observed for all except circularly polarised laser pulses.

The highest energy electrons are subject to relatively few collisions as they pass through thin targets, with thicknesses on the order of ~μm, and emerge from the rear surface. Travelling into the vacuum the electrons cause a space-charge separation leading to an electric field at the target surface, the sheath field. This field reaches sufficiently large magnitudes to result in ionisation of the atoms on the rear surface of the target. Ionisation can also be due to target heating by the electron return current. The newly freed electrons, from the rear surface, are pushed back into the target surface while the ions are accelerated into the vacuum by the sheath field. This is termed target normal sheath acceleration (TNSA) [11] and the direction of the ion beam is normal to the rear surface and the beam is generally found to have a low divergence [12]. These ions are most commonly found to be protons, originating from hydrocarbon contamination layers on the surface of the target, which are preferentially accelerated due to their high charge-mass ratio [4]. Target heating, by radiation or resistive methods, to remove the hydrocarbon layer, has resulted in acceleration of higher Z ions to energies of several MeV [4].

Experimental arrangement

The experiment was performed on the Vulcan laser in Target Area West (TAW). An f/3 off-axis parabola was used to focus the pulse to a FWHM diameter spot of 9.5 μm onto a number of thin foil targets, positioned at ~8° from laser axis. The laser pulse had typical energies of 60 J in a pulse length of 500 fs.

The set of targets were comprised of different materials and thicknesses, including some wedged targets. Target thicknesses ranged from 5-100 μm and were mainly composed of Au, although Cu, foam, Mylar and polypropylene (PP) were also used. Radiochromic film is a dose dependent radiation detector and a stack of film pieces was positioned parallel to the rear surface of the flat targets with a separation of 7 cm between the foil and stack. Figure 1 shows the experimental setup.

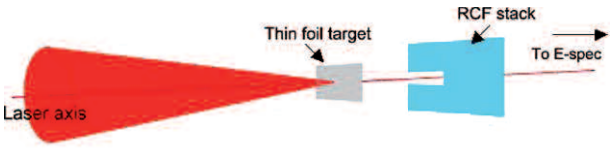

Figure 1. Side view of laser, focused with an f/3 off axis parabola and incident at 8° to the target normal, and radiochromic film stack, situated 7 cm behind the target centred on the target normal and parallel to the front surface of the target.

Protons were detected using a stack of 14, 50×50 mm pieces of RCF: the first eight pieces, labeled A-H, were cut from low sensitivity HD810 film, while the remainder of the stack, I-N, consisted of higher sensitivity MD-55. A thin layer of aluminium foil was used to shield the exposed surfaces of the stack from debris. To allow a clear path for electrons to travel to the electron spectrometer in the laser direction, a 25×4 mm section was removed from the RCF stack. The films were scanned using a flatbed white light scanner and analysis was performed by a Matlab script using only the red channel of the image due to enhanced absorption of the RCF within this spectral range. SRIM2008[13] was used to determine the stopping distances of protons of different energy within the stack. The diagnostic was sensitive to protons within the energy range 1-18 MeV. Energetic protons deposit the bulk of their energy, within their Bragg peak which occurs at the end of their path. It can be assumed that the contribution of a proton of given energy to the a piece of film within the RCF stack will be negligible for all films except the piece in which it is stopped.

Results and discussion

During the experiment wedge targets (figure 2) were also shot. These were aligned so that the front surface normal was always at eight degrees to the laser axis, with the angle between the front and rear surface normals varying from 0 to 35 degrees. The centres of the proton beams generated by these wedged targets were seen to be deflected to a position corresponding to the new rear surface target normal direction. This deflection, which has been found to correspond to the direction of the target rear surface normal, has been noted in previous experiments using wedged targets[1] and provides support that, in this intensity regime, TNSA is the dominant proton acceleration mechanism.

For the flat targets, the RCF exposures show a variety of features. Many demonstrate hollowed beams and ring (figure 3 and figure 4). Clark *et al.*[14] proposed that the annular ring patterns result from the deflection of protons,

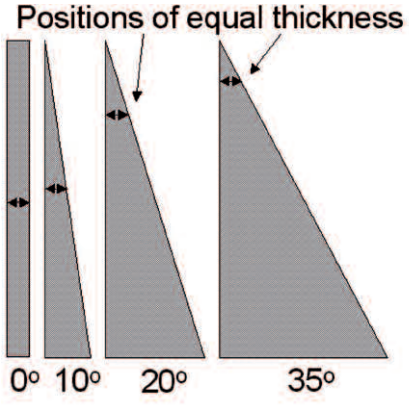

Figure 2. Simple representation of wedged targets.

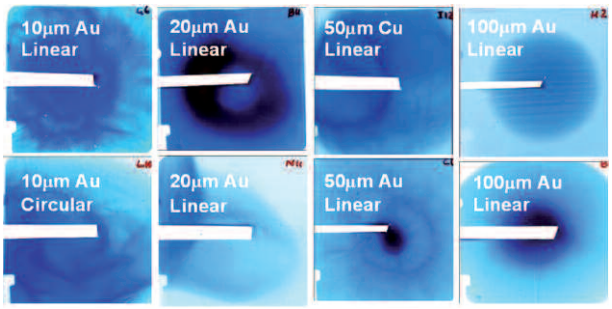

Figure 3. Examples of RCF pieces from a number of different shots. The contrast has been adjusted to aid clarity.

accelerated from the front surface of the 125 μm aluminium targets, in strong magnetic fields within the target. However, it is generally accepted that within the regimes relevant to this experiment the majority of protons are accelerated from the rear surface, here the results from wedge targets support this supposition, and the annular rings are still present.

Hot electrons accelerated from the front of the target, travel collisionlessly through to the rear surface where some escape into the vacuum. This space charge separation leads to the formation of an electrostatic sheath field. Accelerated electrons with insufficient energy to overcome the potential barrier, caused by the sheath field, are reflected back towards the front of the target. On reaching the front surface, again some electrons escape into the vacuum, resulting in a second sheath field at the front of the target. This also reflects electrons. Electrons will continue to be accelerated from the front surface of the target for the duration of the laser pulse. For thin targets it is possible for the recirculated electrons, which have returned to the front surface before the end of the pulse, to return towards the target rear along with surface electrons. The rear field is therefore a superposition of the field due to initially accelerated electrons and that of the recirculated electrons. This results in an increase in the field strength and therefore the peak proton energy and number of accelerated protons[15].

Of the foils considered here the 100 μm targets are only ones in which, for ~500 fs laser pulse, recirculation would be negligible, since the double transit time of relativistic

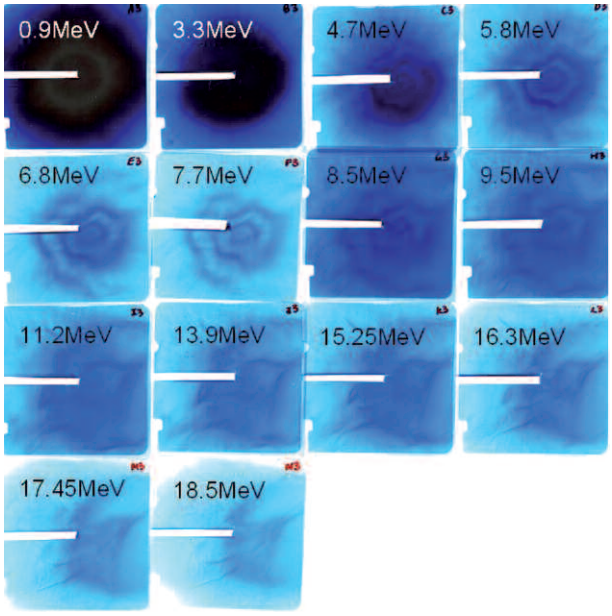

Figure 4. An example of a complete stack, with the film piece closest to the interaction at the top left and the films arranged sequentially left to right, then top to bottom. The given example was exposed to the interaction of a 10 µm target with a linearly polarised pulse. The contrast has been adjusted to aid clarity.

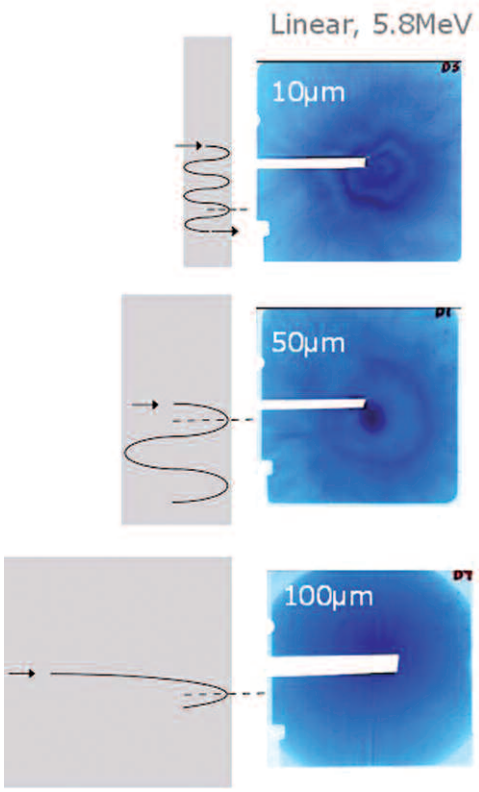

Figure 5. Recirculation within 10 µm and 50 µm targets showing a decrease in number of rings and increase in ring diameter with increasing target thickness. The 100 µm target shows the smooth beam seen in the absence of recirculation.

electrons for this thickness is greater than the pulse duration. Ring patterns are observed in results from all 10, 20 and 50 µm targets regardless of laser polarisation, and are not seen for 100 µm targets.

Figure 5 shows a simplistic model of recirculation, in each case the electron bunch length is the same length as this is dependent on the laser pulse length and the angle of reflection at the rear and front surfaces are approximately the same. In the thinnest target not only are the greatest number of recirculation transits possible but as there is a shorter distance between reflections the separation between the rings is less than in the thicker targets. Each time the electrons reach the rear surface some may have sufficient energy to escape the surface leading to a temporary strengthening of the field in these regions which in turn causes further ionisation and acceleration of the subsequent protons. This is consistent with the trend observed in the raw RCF is that as thickness of the foils increases from 10 to 50 µm fewer rings are visible and the rings are more widely spaced with the inner most ring of the thinnest target having a much smaller radius than the only ring on the 50 µm foil.

Preliminary analysis of the dose data shows a decrease in number of protons as their energy increases, as well as a decrease in average dose, on each film within the stack, with increasing target thickness. The decrease in proton number with increasing proton energy has been observed in a many previous experiments[16,17]. In cases for which TNSA is proposed as the dominant acceleration mechanism, it is thought that the drop in number of accelerated protons is due to a decrease in the strength of the electrostatic sheath field at the rear surface as target thickness increases. Recirculation has been proposed as an explanation because a larger number of recirculations are possible within thinner targets as the double transit time (time for relativistic electrons to travel a distance equivalent to twice the target thickness) is shorter. This allows electrons to recirculate and be reaccelerated by the laser gaining more energy and leading to a stronger surface field than in targets in which recirculation is not possible. As a result a larger number of protons of a higher energy might be expected from targets in which recirculation occurs[17].

The peak proton energy could only be determined for the 100 µm target, where it was found to be 14 MeV. All thinner targets generated protons with energies up to the diagnostic limit of 18 MeV. A reduction in peak proton energy with increasing thickness has been previously documented and is again explained by the reduction in strength of the rear surface sheath field[17]. This is observed for both laser polarisations.

It is expected that a linearly polarised laser pulse will produce higher energy electrons than a circularly polarised pulse with the same peak intensity. This is due to the suppression of J×B heating in circularly polarised light. The near normal incidence of the laser minimises vacuum heating, which results from electrons being accelerated into the plasma by a component of the electric field normal to the target surface, for both polarisations, while the J×B heating is close to optimal. No significant difference in proton signal was measured between linearly and circularly

polarised laser pulses for any target. If anything the variation between the signals became less as the target thickness increased.

Conclusion

Beam deflection using wedge targets confirmed TNSA as the dominant mechanism.

Using RCF, annular rings were observed within the proton beam profile, which appear to be related to recirculation. Recirculation may have a significant effect upon the sheath field created at the rear surface of the target. As well as the ring features, the increase in number of accelerated protons and peak proton energy with decreasing target thickness can be explained by changes in the rear surface sheath field due to an increase in recirculation of hot electrons within the target.

Acknowledgements

The authors would like to acknowledge the help of their collaborators as well as the vital assistance of the Vulcan operations team throughout this experiment.

References

1. R. A. Snavely *et al.*, *Phys. Rev. Lett.* **85**, 2945-2948 (2000).
2. M. Borghesi *et al.*, *Phys., Rev. Lett.* **88**, 135002 (2002).
3. Y. I. Salamin *et al.*, *Phys. Rev. Lett.* **100**, 155004 (2008).
4. M. Hegelich *et al.*, *Phys. Rev. Lett.* **89**, 085002 (2002).
5. H. Schwoerer *et al.*, *Nature* **439**, 445 (2006).
6. A. P. L. Robinson *et al.*, *Phys. Rev. Lett.* **96**, 035005 (2006).
7. L. O. Silva *et al.*, *Phys. Rev. Lett.* **92**, 015002 (2004).
8. A. Maksimchuk *et al.*, *Phys. Rev. Lett.* **84**, 4108-4111 (2000).
9. S. C. Wilks and W. L. Kruer, *IEEE J. Quant. Elec.* **33**, 1954-1968 (1997).
10. Y. Ping *et al.*, *Phys. Rev. Lett.* **100**, 085004 (2008).
11. S. C. Wilks *et al.*, *Physics of Plasmas* **8**, 542 (2001).
12. S. Ter-Avetisyan *et al.*, *Phys. Rev. E* **77**, 016403 (2008).
13. Ziegler, http://www.srim.org/SRIM/SRIM2008.htm
14. E. L. Clark *et al.*, *Phys. Rev. Lett.* **84**, 670 (2000).
15. Y. Sentoku *et al.*, *Phys. Plasmas* **10**, 2009-2015 (2003).
16. J. Fuchs *et al.*, *Phys. Rev. Lett.* **94**, 045004 (2005).
17. A. Mackinnon *et al.*, *Phys. Rev. Lett.* **88**, 215006 (2002).